Limitations of the pseudo-Newtonian approach in studying the accretion flow around a Kerr black hole

Indu K. Dihingia,[†] Santabrata Das,[*] Debaprasad Maity,[‡] and Sayan Chakrabarti[§]
Department of Physics, Indian Institute of Technology Guwahati, Guwahati 781039, Assam, India

(Received 28 June 2018; published 8 October 2018)

We study the relativistic accretion flow in a generic stationary axisymmetric space-time and obtain an effective potential ($\Phi^{\rm eff}$) that accurately mimics the general relativistic features of Kerr black hole having spin $0 \le a_{\rm k} < 1$. Considering the accretion disc to be confined around the equatorial plane of a rotating black hole and using the relativistic equation of state, we examine the properties of the relativistic accretion flow and compare them with the same obtained form semirelativistic as well as nonrelativistic accretion flows. Towards this, we first investigate the transonic properties of the accretion flow around the rotating black hole where good agreement is observed for relativistic and semirelativistic flows. Further, we study the nonlinearities such as shock waves in accretion flow. Here also we find that the shock properties are in agreement for both relativistic and semirelativistic flows irrespective of the black hole spin ($a_{\rm k}$), although it deviates significantly for nonrelativistic flow. In fact, when the particular shocked solutions are compared for flows with identical outer boundary conditions, the positions of shock transition in relativistic and semirelativistic flows agree well with the deviation of 6%–12% for $0 \le a_{\rm k} \le 0.99$, but vast disagreement is observed for nonrelativistic flow. In addition, we compare the parameter space [in energy ($\mathcal{E}$) and angular momentum (λ) plane] for shock to establish the fact that relativistic as well as semirelativistic accretion flow dynamics do show close agreement irrespective of $a_{\rm k}$ values, whereas nonrelativistic flow fails to do so. With these findings, we point out that semirelativistic flow including $\Phi^{\rm eff}$ satisfactorily mimics the relativistic accretion flows around the Kerr black hole. Finally, we discuss the possible implications of this work in the context of dissipative advective accretion flow around Kerr black holes.

DOI: 10.1103/PhysRevD.98.083004

I. INTRODUCTION

The accretion of matter on to a black hole is considered to be an essential physical phenomenon as it is regarded to be the principal source of power in microquasars, active galactic nuclei, and quasars [1]. The overall description through which one studies the accretion process is the hydrodynamic flow of matter in the background of black hole space-time. Indeed, when inflowing matter approaches towards the horizon, the general relativistic (GR) effects become important and due to nonlinearity, it is, in general, difficult to solve the problem. To avoid complexity, therefore, most of the studies of accretion flow around black holes were confined in the Newtonian regime where gravitational effect is taken into account using effective potentials. In practice, while studying accretion dynamics, people conventionally adopt some trial effective potentials known as pseudo-Newtonian potentials that approximately mimic the general relativistic effects around the black hole. This evidently yields erroneous results particularly when one studies the physical processes in the vicinity of the black hole. Therefore, the search for an effective potential that accurately describes the space-time geometry around the black hole is very much appealing although it is an age old endeavor in the context of the black hole accretion process and in this work, we attempt to do so.

In the case of accretion around Schwarzschild black holes, the pseudo-Newtonian potential was first proposed by Paczyńsky and Wiita [2] (hereafter PW80), which provides very satisfactory results. Numerous groups of researchers extensively investigated the physical properties of the astrophysical flows around nonrotating black holes using PW80 potential [[3–17] and references therein].

However, in reality, the presumption of nonrotating black holes is possibly too simplistic in the sense that all the cosmological objects are expected to be rotating. Hence, the use of Kerr geometry as an appropriate background seems to be inevitable, which, in general, plays a key role in studying the accretion phenomenon around rotating black holes. However, solving the GR

[*]Corresponding author.
sbdas@iitg.ac.in
[†]i.dihingia@iitg.ac.in
[‡]debu@iitg.ernet.in
[§]sayan.chakrabarti@iitg.ac.in

hydrodynamic equations around a Kerr black hole is complicated and challenging. To overcome this, various pseudopotentials for Kerr black hole were proposed [18–23]. All these potentials were prescribed based on certain physical constraints and the problem under consideration. Naturally, all of them have their own limitations and therefore, the regime of validity of these potentials is very much restricted. For example, the potential proposed by [20] describes the space-time geometry satisfactorily for the black hole spin parameter $a_{\rm k} < 0.8$ and thus, this potential cannot be used to study the systems which are believed to harbor rapidly rotating black holes like Sgr A*, Cyg X-1, LMC X-1, M33 X-7, 4U 1543-47, GRO J1655-40, GX 339-4, etc. [24–29]. Therefore, it is of prime importance in the astrophysical context to ascertain the form of the effective potential corresponding to a Kerr black hole, which will be free from any *a priori* restrictions mentioned above.

With the increasing sophistication of observational techniques and precession measurements, it would always be prudent to understand any physical phenomena in a model independent way. For example, in the weak gravity regime, Einstein's theory has been proven to be very successful through a large number of observations. Although the high precession measurement in the strong gravity regime is yet to be substantiated, it has the potential to differentiate new physics beyond Einstein, if any. Keeping this in mind, our goal in this paper will be multifold. First, to make our analysis model independent, we will be considering a generic axisymmetric space-time, and then formulating the full general relativistic hydrodynamics. While studying different component equations of the hydrodynamics, it turns out that in the static limit, the radial flow equation can be cast into a Newtonian-like flow equation. Therefore, the most powerful result we obtain through the present analysis is an analytic expression for the effective potential for any generic axisymmetric black hole space-time. Next, we consider the Kerr metric as a representation of the rotating black hole and study the accretion dynamics in detail. In continuation, we infer the limitations of the conventional Newtonian approach while examining the accretion flow around the black holes in the nonrelativistic limit using effective potentials. To this end, we mention some of the recent important theoretical developments in the nonrelativistic hydrodynamics as a special limit of relativistic hydrodynamics for certain conformal field theory. In the slow fluid velocity limit (i.e., $v/c \ll 1$), when the fluid pressure is redefined in a way that the thermal motion of the fluid constituents do not violate the above speed limit, the relativistic hydrodynamic equations for a conformal field theory boil down to the incompressible nonrelativistic Navier-Stokes equation [30]. Soon after, Bhattacharyya, Minwalla, and Wadia [31] reported similar findings by appropriately scaling all fluid and thermodynamic variables, respectively.

In this work, we are also interested to the similar nonrelativistic limit. In fact, our goal is to move even further where we quantitatively compare the results obtained from different limits, such as relativistic (R) and nonrelativistic [NR; $v/c \ll 1$ and $k_B T/(m_e c^2) \ll 1$] specifically in the context of accretion flow dynamic. The most important findings we observe here is that the conventional Newtonian approach to study the accretion flow around the black hole endures inherent limitation that originates due to the adopted deceiving dynamics of the flow in the vicinity of the black hole horizon. Moreover, we confer the essence of these differences exclusively focusing the relativistic effect on the flow dynamics.

For simplicity, we consider an adiabatic advective accretion flow to obtain the effective potential for a rotating black hole. The conservation equations that govern the dynamics of the accretion flow around the rotating black hole are the mass conservation equation, the radial momentum conservation equation, and the entropy generation equation, respectively. By suitably defining the radial three-velocity (v) in a corotating frame, the radial momentum equation is expressed as the addition of three terms, namely, kinetic energy, thermal energy, and gravitation energy, respectively, at per with the Newtonian flow equation although all the conserved equations under consideration are fully relativistic in nature. With this, we successfully identify the analytic expression of the effective potential in a generic axisymmetric space-time.

In view of the importance of the effective potential, we intend to investigate the behavior of accretion flow around a rotating black hole. We find the global transonic solutions that connect the black hole horizon and the outer edge of the disc (equivalently large distance away from the black hole). In reality, during accretion, rotating matter is piled up in the vicinity of the black hole due to the centrifugal repulsion against gravity that eventually triggers the discontinuous transition of the flow variables in the form of a shock wave [5,9,10,16,17,32–37]. We calculate the global transonic accretion solutions including shock waves and compare them for all the limiting conditions considering nonrotating, weakly rotating, and rapidly rotating black holes. Further, we separate the domain of the parameter space in the angular momentum and energy ($\lambda - \mathcal{E}$) plane according to the nature of flow solutions. We also identify the effective region of the parameter space for a wide range of black hole spin values that admits shock induced global accretion solutions. In this work, we ignore the dissipative processes, namely, viscosity, radiative cooling, and magnetic fields to avoid complexity. We plan to consider these physical processes in the future study.

In Sec. II, we discuss the mathematical background. In Sec. III, we describe the governing equations and carry out the critical point analysis. In Sec. IV, we discuss the global accretion solutions with and without shocks and also classify the shock parameter space. Finally, in Sec. V, we present concluding remarks.

II. RELATIVISTIC HYDRODYNAMICS IN GENERAL STATIONARY AXISYMMETRIC SPACE-TIME

As emphasized earlier, we analyze the relativistic hydrodynamic equations in a generic stationary axisymmetric space-time. The defining property of a static axisymmetric space-time is the existence of two commuting killing vectors which we will take along (t, ϕ) direction. The rest of the spacelike coordinates identified as (r, θ) will be assumed to be mutually orthogonal as well as orthogonal to the two killing vector fields at each point in the space-time. Therefore, with the above choice of the coordinate system a generic stationary axisymmetric space-time can be expressed as

$$\begin{aligned} ds^2 &= g_{\mu\nu} dx^\mu dx^\nu \\ &= g_{tt} dt^2 + 2 g_{t\phi} dt d\phi + g_{\phi\phi} d\phi^2 + g_{rr} dr^2 + g_{\theta\theta} d\theta^2, \end{aligned} \tag{1}$$

where μ and ν are indices that run from 0 to 3. Assuming a black hole to be located at the center, the horizon is identified as $g^{rr} = 1/g_{rr} = 0$. Because of the two killing vectors $(l_t = \partial_t, l_\phi = \partial_\phi)$, all the metric coefficients will, in general, be a function of (r, θ).

A. Hydrodynamics

Hydrodynamics is a model independent approach towards the understanding of the low energy dynamics of any generic field theory. The construction is based on the underlying symmetry and the associated conservation laws of the theory. If we consider a Lorentz invariant theory with a global $U(1)$ symmetry, properties of hydrodynamic flow are studied using the following two conservation equations for the energy-momentum and particle number:

$$T^{\mu\nu}_{;\nu} = 0 \quad \text{and} \quad j^\mu_{;\mu} = 0. \tag{2}$$

Here, the energy-momentum tensor $T^{\mu\nu}$ and the particle number current j^μ are expressed in terms of systematic derivative expansion of the fluid degrees of freedom consisting of local energy density $e(r)$, pressure $p(r)$, and the four velocity u^μ supplemented by the condition $u^\mu u_\mu = -1$. In general, one writes

$$T^{\mu\nu} = T^{\mu\nu}_0 + \pi^{\mu\nu} \quad \text{and} \quad j^\mu = j^\mu_0 + \pi^\mu. \tag{3}$$

These equations (3) are called constitutive relations. The first term in the right-hand side of both equations is zeroth order, and the second term contains all derivative terms. For example, the dissipative term which contains the first order derivative in fluid velocity will appear in the second term. For the present analysis, we confine ourself only to the zeroth order term. Therefore, zeroth order expansion of the energy-momentum tensor and the four current are written as

$$T^{\mu\nu}_0 = (e + p) u^\mu u^\nu + p g^{\mu\nu} \quad \text{and} \quad j^\mu_0 = \rho u^\mu, \tag{4}$$

where e, p, and ρ are the local energy density, local isotropic pressure, and mass density of the flow. Therefore, the final zeroth order hydrodynamic equations are given by

$$T^{\mu\nu}_{0\ ;\nu} = 0 \quad \text{and} \quad (\rho u^\nu)_{;\nu} = 0. \tag{5}$$

With respect to the fluid flow, we construct the projection operator $h^i_\mu = \delta^i_\mu + u^i u_\mu$, where "$i$" takes (1,2,3) values. It also satisfies $h^i_\mu u^\mu = 0$. This condition helps us to project the Navier-Stokes equation into three vector equations as

$$h^i_\mu T^{\mu\nu}_{0\ ;\nu} = (e + p) u^\nu u^i_{;\nu} + (g^{i\nu} + u^i u^\nu) p_{,\nu} = 0, \tag{6}$$

and a scalar equation which is essentially identified as first law of thermodynamics,

$$u_\mu T^{\mu\nu}_{;\nu} = u^\mu \left[\left(\frac{e + p}{\rho} \right) \rho_{,\mu} - e_{,\mu} \right] = 0. \tag{7}$$

In this work, our goal is to cast the relativistic radial momentum flow equation at par with the Newtonian-like equation. Therefore, we define the following variables in their appropriate form: the angular velocity variable $v_\phi^2 = (u^\phi u_\phi)/(-u^t u_t)$, and the associated bulk azimuthal Lorentz factor as $\gamma_\phi^2 = 1/(1 - v_\phi^2)$. Subsequently, the polar three-velocity is defined as $v_\theta^2 = \gamma_\phi^2 (u^\theta u_\theta)/(-u^t u_t)$ and the associated bulk polar Lorentz factor as $\gamma_\theta^2 = 1/(1 - v_\theta^2)$. Similarly, the radial three-velocity in the corotating frame is defined as $v^2 = \gamma_\phi^2 \gamma_\theta^2 v_r^2$, where $v_r^2 = (u^r u_r)/(-u^t u_t)$ and the associated bulk radial Lorentz factor as $\gamma_v^2 = 1/(1 - v^2)$. Employing these definitions of the velocities in Eq. (6), we obtain the equations corresponding to $i = r$ and $i = \theta$ which are given by

$$\begin{aligned} &\gamma_v^2 v \frac{\partial v}{\partial r} + \gamma_v^2 \gamma_\theta v_\theta \sqrt{\frac{g_{rr}}{g_{\theta\theta}}} \frac{\partial v}{\partial \theta} + \frac{\gamma_\theta v v_\theta}{2\sqrt{g_{rr} g_{\theta\theta}}} \frac{\partial g_{rr}}{\partial \theta} - \frac{v_\theta^2 \gamma_\theta^2}{2 g_{\theta\theta}} \frac{\partial g_{\theta\theta}}{\partial r} \\ &\quad + \frac{1}{e + p} \frac{\partial p}{\partial r} + \frac{\gamma_\theta v v_\theta}{e + p} \sqrt{\frac{g_{rr}}{g_{\theta\theta}}} \frac{\partial p}{\partial \theta} + \gamma_\theta^2 \frac{\partial \Phi^{\mathrm{eff}}}{\partial r} = 0, \end{aligned} \tag{8}$$

and

$$\begin{aligned} &\gamma_\theta^3 v \frac{\partial v_\theta}{\partial r} + \gamma_\theta^4 v_\theta \sqrt{\frac{g_{rr}}{g_{\theta\theta}}} \frac{\partial v_\theta}{\partial \theta} + \gamma_v^2 \gamma_\theta v^2 v_\theta \frac{\partial v}{\partial r} \\ &\quad + \gamma_v^2 \gamma_\theta^2 v v_\theta^2 \sqrt{\frac{g_{rr}}{g_{\theta\theta}}} \frac{\partial v}{\partial \theta} - \frac{v}{2} \sqrt{\frac{g_{rr}}{g_{\theta\theta}}} \left(\frac{v}{g_{rr}} \frac{\partial g_{rr}}{\partial \theta} - \frac{\gamma_\theta v_\theta}{\sqrt{g_{rr} g_{\theta\theta}}} \frac{\partial g_{\theta\theta}}{\partial r} \right) \\ &\quad + \frac{\gamma_\theta^2 - v^2}{e + p} \sqrt{\frac{g_{rr}}{g_{\theta\theta}}} \frac{\partial p}{\partial \theta} + \frac{\gamma_\theta v v_\theta}{e + p} \frac{\partial p}{\partial r} + \gamma_\theta^2 \sqrt{\frac{g_{rr}}{g_{\theta\theta}}} \frac{\partial \Phi^{\mathrm{eff}}}{\partial \theta} = 0. \end{aligned} \tag{9}$$

As already mentioned, the defining property of a general static, axisymmetric space-time is the existence of two commuting Killing vector fields, $l^\mu_t \equiv \partial_t$ and $l^\mu_\phi \equiv \partial_\phi$, associated with time translation and azimuthal rotation, respectively. For each globally defined killing vector l there exists an associated conserved quantity, say Q_l. By using the equations for the mass and energy-momentum conservations, in general, for a nondissipative fluid, one can express the aforementioned conserved quantity $Q_l = l^\mu h u_\mu$, which satisfies the conservation equation $\pounds_u Q_l = 0$, where $\pounds_u$ is the Lie derivative along the flow vector u. Hence, the fluid flow around a static, axisymmetric background leads to the following two conserved quantities:

$$hu_\phi = \mathcal{L}(\text{constant}) \quad \text{and} \quad hu_t = \mathcal{E}(\text{constant}), \tag{10}$$

where $h[= (e+p)/\rho]$ is the enthalpy of the flow and $\mathcal{E}$ is the relativistic Bernoulli constant. Here, $u_t^2 = \gamma^2/(g^{t\phi}\lambda - g^{tt})$, where $\lambda = -u_\phi/u_t$ is the conserved specific angular momentum of the fluid and $\gamma = \gamma_\phi\gamma_v\gamma_\theta$ is the total bulk Lorentz factor. It is to be noted that Eqs. (8) and (9) exactly reduce to the Euler equations of the Newtonian hydrodynamics (follow [38]). Thus, these two equations describe the relativistic momentum of the flow along radial (r) and polar (θ) directions where $\Phi^{\rm eff}$ denotes the effective pseudopotential and is given by

$$\Phi^{\rm eff} = 1 + 0.5\ln(\Phi), \tag{11a}$$

where

$$\Phi = \frac{g_{t\phi}^2 - g_{tt}g_{\phi\phi}}{g_{\phi\phi} + 2\lambda g_{t\phi} + \lambda^2 g_{tt}}. \tag{11b}$$

In the next section, we consider a specific black hole background of astrophysical interest and discuss its consequence on the accretion flow dynamics in detail.

III. GOVERNING EQUATIONS

A. Equations describing relativistic accretion flow around the Kerr black hole

In the present paper, we consider a specific stationary axisymmetric space-time for the Kerr black hole. In terms of Boyer-Lindquist coordinates, the components of the Kerr metric are expressed as follows [39]:

$$g_{tt} = -\left(1 - \frac{rr_g}{\Sigma}\right); \qquad g_{t\phi} = -\frac{a_{\rm k} r r_g \sin^2\theta}{\Sigma}$$
$$g_{rr} = \frac{\Sigma}{\Delta}; \qquad g_{\theta\theta} = \Sigma; \qquad g_{\phi\phi} = \frac{A\sin^2\theta}{\Sigma}, \tag{12}$$

where $A = (r^2 + a_{\rm k}^2)^2 - \Delta a_{\rm k}^2 \sin^2\theta$, $\Sigma = r^2 + a_{\rm k}^2\cos^2\theta$ and $\Delta = r^2 - r_g r + a_{\rm k}^2$, respectively. This metric successfully describes the space-time geometry around a rotating black hole of mass $M_{\rm BH}$ and angular momentum J. We write the specific spin of the black hole as $a_{\rm k} = J/M_{\rm BH}$. For convenience, we use a unit system as $G = M_{\rm BH} = c = 1$, where G and c are the gravitational constant and speed of light. Therefore, measurements of speed, mass, length, time, angular momentum, and energy will be expressed in units of c, $M_{\rm BH}$, $GM_{\rm BH}/c^2$, $GM_{\rm BH}/c^3$, $GM_{\rm BH}/c$ and $M_{\rm BH}c^2$, respectively. It is to be noted that in Eq. (12), r_g refers the Schwarzchild radius and is given by $r_g = 2GM_{\rm BH}/c^2$. In this unit system, the effective potential around a Kerr black hole is computed as

$$\Phi^{\rm eff} = 1 + \ln\left[\frac{A(2r - \Sigma)\sin^2\theta - 4a_{\rm k}^2 r^2 \sin^4\theta}{\Sigma\lambda(\lambda\Sigma + 4a_{\rm k} r\sin^2\theta - 2\lambda r) - A\Sigma\sin^2\theta}\right]. \tag{13}$$

In this work, our goal is to solve the hydrodynamic equations around the Kerr black hole. In order to proceed further, we consider a geometrically thin accretion disc which is confined around the black hole equatorial plane. Therefore, for simplicity, we choose $\theta = \pi/2$. Accordingly, the flow motion along the transverse direction is considered to be negligible, i.e., $v_\theta = 0$. With this, we have $\gamma_\theta = 1$ and $u_t = \gamma_v\sqrt{\frac{r\Delta}{a_{\rm k}^2(r+2) - 4a_{\rm k}\lambda + r^3 - \lambda^2(r-2)}}$. Moreover, we also neglect the θ variation of all the flow variables. With these approximations, the radial component of Eq. (8) turns out to be the well-known Navier-Stokes equation, which is given by

$$v\gamma_v^2\frac{dv}{dr} + \frac{1}{h\rho}\frac{dp}{dr} + \frac{d\Phi_e^{\rm eff}}{dr} = 0, \tag{14}$$

where $\Phi_e^{\rm eff}$ represents the effective pseudopotential calculated at the equatorial plane ($\theta = \pi/2$) and is given by

$$\Phi_e^{\rm eff} = 1 + \frac{1}{2}\ln\left[\frac{r\Delta}{a_{\rm k}^2(r+2) - 4a_{\rm k}\lambda + r^3 - \lambda^2(r-2)}\right]. \tag{15}$$

Similarly, the entropy generation equation is calculated from Eq. (7) as

$$\left(\frac{e+p}{\rho}\right)\frac{d\rho}{dr} - \frac{de}{dr} = 0. \tag{16}$$

The second part of Eq. (5), which is basically the continuity equation, is rewritten in an integrated form as

$$\dot{M} = -4\pi v\gamma_v \rho H\sqrt{\Delta}, \tag{17}$$

where $\dot{M}$ is the accretion rate and H is the local half-thickness of the disc and its functional form under thin disc approximation is computed as [40,41]

$$H^2 = \frac{pr^3}{\rho \mathcal{F}}, \qquad \mathcal{F} = \gamma_\phi^2 \frac{(r^2 + a_{\rm k}^2)^2 + 2\Delta a_{\rm k}^2}{(r^2 + a_{\rm k}^2)^2 - 2\Delta a_{\rm k}^2}. \tag{18}$$

In order to solve Eqs. (14), (16), and (17), one needs to consider a relation among e, ρ, and p, commonly known as equation of state (EOS). In the subsequent analysis, we adopt an EOS proposed by [42] that agrees quite satisfactorily with the exact EOS of the fluid [43–45]. For a fluid consisting of electrons, positrons, and ions, the EOS is given by

$$e = n_e m_e f = \frac{\rho}{\tau} f, \tag{19}$$

where $\rho = n_e m_e \tau$ and $\tau = [2 - \xi(1 - 1/\chi)]$. Here, n_e (n_p) and m_e (m_p) represent the number density and mass of the electron (ion). Moreover, we define $\xi = n_p/n_e$ and $\chi = m_e/m_p$, respectively. Throughout our study, we use $\xi = 1$, until otherwise stated. Finally, the functional form of f is given by

$$f = (2-\xi)\left[1 + \Theta\left(\frac{9\Theta + 3}{3\Theta + 2}\right)\right] + \xi\left[\frac{1}{\chi} + \Theta\left(\frac{9\Theta + 3/\chi}{3\Theta + 2/\chi}\right)\right], \tag{20}$$

where we define the dimensionless temperature of the fluid as $\Theta = k_B T/m_e c^2$. In addition, the polytropic index (N), specific heat ratio (Γ), and sound speed (C_s) are defined as

$$N = \frac{1}{2}\frac{df}{d\Theta}; \quad \Gamma = 1 + \frac{1}{N} \quad \text{and} \quad C_s^2 = \frac{\Gamma p}{e + p} = \frac{2\Gamma\Theta}{f + 2\Theta}. \tag{21}$$

After some algebraic steps involving Eqs. (14), (16), (17), and (19), we calculate the wind equation as

$$\frac{dv}{dr} = \frac{\mathcal{N}_{\rm R}}{\mathcal{D}_{\rm R}}, \tag{22}$$

where denominator $\mathcal{D}_{\rm R}$ is given by

$$\mathcal{D}_{\rm R} = \gamma_v^2\left[v - \frac{2C_s^2}{v(\Gamma + 1)}\right], \tag{23}$$

and numerator $\mathcal{N}_{\rm R}$ is given by

$$\mathcal{N}_{\rm R} = \frac{2C_s^2}{\Gamma + 1}\left[\frac{(r - a_{\rm k}^2)}{r\Delta} + \frac{5}{2r} - \frac{1}{2\mathcal{F}}\frac{d\mathcal{F}}{dr}\right] - \frac{d\Phi_e^{\rm eff}}{dr}. \tag{24}$$

Similarly, the gradient of the temperature is obtained as

$$\frac{d\Theta}{dr} = -\frac{2\Theta}{2N + 1}\left[\frac{(r - a_{\rm k}^2)}{r\Delta} + \frac{\gamma_v^2}{v}\frac{dv}{dr} + \frac{5}{2r} - \frac{1}{2\mathcal{F}}\frac{d\mathcal{F}}{dr}\right]. \tag{25}$$

In Eqs. (24) and (25), the logarithmic derivatives of $\mathcal{F}$ is calculated as

$$\frac{1}{\mathcal{F}}\frac{d\mathcal{F}}{dr} = \gamma_\phi^2 \lambda \Omega' + 4a_{\rm k}^2(a_{\rm k}^2 + r^2)\frac{(a_{\rm k}^2 + r^2)\Delta\prime - 4r\Delta}{(a_{\rm k}^2 + r^2)^4 - 4a_{\rm k}^4\Delta^2}, \tag{26}$$

where $\Delta' = 2(r - 1)$ and

$$\Omega' = -2\frac{a_{\rm k}^3 - 2a_{\rm k}^2\lambda + a_{\rm k}(\lambda^2 + 3r^2) + \lambda(r - 3)r^2}{(a_{\rm k}^2(r + 2) - 2a_{\rm k}\lambda + r^3)^2}. \tag{27}$$

It is to be noted that the ratio of the radial flow velocity (v) to the speed of light (c) always remains $v/c \lesssim 0.1$ even in the region $r > 4r_g$ ([46], and references therein). Therefore, for all practical purpose, we can safely set $\gamma_v \to 1$ and hence, the radial momentum equation (14) reduces into the simplified form as

$$v\frac{dv}{dr} + \frac{1}{h\rho}\frac{dp}{dr} + \frac{d\Phi_e^{\rm eff}}{dr} = 0. \tag{28}$$

However, it would be worthy to compare results obtained separately using Eqs. (14) and (28) which will be discussed in the subsequent sections. For convenience, we refer to the analysis that incorporates Eq. (28) as a semirelativistic (SR) limit.

B. Equations in the nonrelativistic limit

A nonrelativistic accretion flow is characterized by $v \ll 1$ all throughout. Therefore, in this limit, the Lorentz factor becomes $\gamma_v = 1$. Moreover, one also needs to maintain the temperature and pressure of the fluid, so that thermal speed should not exceed the nonrelativistic limit (i.e., $\Theta \ll 1$). With this consideration, the enthalpy of the flow becomes $h(r) \sim 1$ and hence, $(h\rho)^{-1}(dp/dr) \sim \rho^{-1}(dp/dr)$. With this, the radial momentum equation is reduced as

$$v\frac{dv}{dr} + \frac{1}{\rho}\frac{dp}{dr} + \frac{d\Phi_e^{\rm eff}}{dr} = 0. \tag{29}$$

It may be noted that Eq. (29) is the well-known Euler equation in Newtonian hydrodynamics. Upon integrating Eq. (29), we obtain the specific energy (including the rest mass energy) of the flow as

$$\mathcal{E}_{\rm NR} = \frac{v^2}{2} + h + \Phi_e^{\rm eff} - 1, \tag{30}$$

where we use the relation $\rho^{-1}(dp/dr) = dh/dr$. Now, it is clear that in the nonrelativistic limit, the radial momentum equation transforms into the Newtonian hydrodynamics equations with an effective potential $\Phi_e^{\rm eff}$. In the limit $r \gg 2$, Eq. (15) reduces to the Newtonian effective potential experienced by a particle around a Newtonian object and is given by

$$\Phi_e^{\rm eff}|_{r\gg 2} = \Phi_{\rm Newton} = 1 - \frac{1}{r} + \frac{\lambda^2}{2r^2}.$$

Needless to mention that the entropy generation equation [Eq. (16)] and the mass conservation equation [Eq. (17)] remain unaltered in the nonrelativistic domain. Using Eqs. (16), (17), and (29), we again calculate the wind equation which is given by

$$\frac{dv}{dr} = \frac{\mathcal{N}_{\rm NR}}{\mathcal{D}_{\rm NR}}, \tag{31}$$

where denominator $\mathcal{D}_{\rm NR}$ is given by

$$\mathcal{D}_{\rm NR} = \left[v - \frac{2C_s^2 h}{v(\Gamma+1)}\right], \tag{32}$$

and numerator $\mathcal{N}_{\rm NR}$ is given by

$$\mathcal{N}_{\rm NR} = \frac{2C_s^2 h}{(\Gamma+1)}\left[\frac{(r-a_{\rm k}^2)}{r\Delta} + \frac{5}{2r} - \frac{1}{2\mathcal{F}}\frac{d\mathcal{F}}{dr}\right] - \frac{d\Phi_e^{\rm eff}}{dr}. \tag{33}$$

Here, subscript "NR" denotes the quantities calculated considering the nonrelativistic approximation.

The gradient of the temperature is computed as

$$\frac{d\Theta}{dr} = -\frac{2\Theta}{2N+1}\left[\frac{(r-a_{\rm k}^2)}{r\Delta} + \frac{1}{v}\frac{dv}{dr} + \frac{5}{2r} - \frac{1}{2\mathcal{F}}\frac{d\mathcal{F}}{dr}\right]. \tag{34}$$

In the subsequent sections, we carry out the comparative analysis considering relativistic, semirelativistic, and nonrelativistic equations, and show how the flow properties obtained from nonrelativistic hydrodynamics significantly deviate from those computed from relativistic dynamics specifically near the black hole horizon.

C. Critical point analysis

During the course of accretion around the black hole, flow starts to move inwards subsonically from the outer edge of the disc and eventually enters into the black hole with supersonic speed. Since the flow accretes smoothly along the streamline, the radial velocity gradient remains real and finite always. However, Eqs. (23) and (32) indicate that the denominator ($\mathcal{D}_{\rm R}$ and $\mathcal{D}_{\rm NR}$) of the wind equations may vanish at some radial coordinate. To maintain the smoothness of the flow, the numerator ($\mathcal{N}_{\rm R}$ and $\mathcal{N}_{\rm NR}$) of the wind equations must also go to zero there. Such a special point where the gradient of the radial velocity takes the form as $(dv/dr)_{\rm c} \to 0/0$ is called a critical point (r_c). Setting the numerator and denominator simultaneously equal to zero, we obtain the critical point conditions which are given below for both relativistic and nonrelativistic cases.

1. Critical point conditions for relativistic flow

For the relativistic flow, setting $\mathcal{D}_{\rm R} = 0$ in Eq. (23), we obtain the radial velocity ($v_{\rm c}$) at the critical point ($r_{\rm c}$) as

$$v_{\rm c}^2 = \frac{2C_{sc}^2}{(\Gamma_{\rm c}+1)}. \tag{35}$$

Further, setting $\mathcal{N}_{\rm R} = 0$ in Eq. (24), we get the sound speed (C_{sc}) at $r_{\rm c}$ as

$$C_{sc}^2 = \frac{\Gamma_{\rm c}+1}{2}\left(\frac{d\Phi_e^{\rm eff}}{dr}\right)_{\rm c}\left[\frac{(r_{\rm c}-a_{\rm k}^2)}{r_{\rm c}\Delta_{\rm c}} + \frac{5}{2r_{\rm c}} - \frac{1}{2\mathcal{F}_{\rm c}}\frac{d\mathcal{F}_{\rm c}}{dr}\right]^{-1}. \tag{36}$$

2. Critical point conditions for the nonrelativistic flow

For the nonrelativistic flow, setting $\mathcal{D}_{\rm NR} = 0$ in Eq. (32), we calculate the radial velocity ($v_{\rm c}$) at $r_{\rm c}$ as

$$v_{\rm c}^2 = \frac{2C_{sc}^2 h_{\rm c}}{(\Gamma_{\rm c}+1)}. \tag{37}$$

As before, we set $\mathcal{N}_{\rm NR} = 0$ in Eq. (33) to get the sound speed at the critical point as

$$C_{sc}^2 = \frac{\Gamma_{\rm c}+1}{2h_{\rm c}}\left(\frac{d\Phi_e^{\rm eff}}{dr}\right)_{\rm c}\left[\frac{(r_{\rm c}-a_{\rm k}^2)}{r_{\rm c}\Delta_{\rm c}} + \frac{5}{2r_{\rm c}} - \frac{1}{2\mathcal{F}_{\rm c}}\frac{d\mathcal{F}_{\rm c}}{dr}\right]^{-1}. \tag{38}$$

In the above, subscript "c" refers the flow variables at $r_{\rm c}$. Since the gradient of the radial velocity takes the "0/0" form at $r_{\rm c}$, we apply the l' Hospital rule to calculate $dv/dr|_{\rm c}$ at $r_{\rm c}$, which is given by

$$\left.\frac{dv}{dr}\right|_{\rm c} = \frac{-B \pm \sqrt{B^2 - 4AC}}{2A}. \tag{39}$$

In Eq. (39), A, B, and C are functions of flow variables and their explicit expressions are given in Appendix A. As it is already pointed out that accretion solutions around the black hole must be transonic in nature, flow must contain at least one critical point [3,47]. Depending on the input parameters, accretion flow may possess multiple critical points as well. When both values of $(dv/dr)_{\rm c}$ are real with opposite sign, the critical point is called as a saddle type and when $(dv/dr)_{\rm c}$ becomes imaginary, the point is called an "O"-type critical point. It may be noted that when $(dv/dr)_{\rm c}$ is negative, it corresponds to the accretion solution and the positive $(dv/dr)_{\rm c}$ yields the wind solution. In this work, we are interested to accretion solutions only and therefore, we keep the wind solutions aside for future study.

IV. RESULTS

A. Computation of critical points

The procedure to calculate the critical point location in all kinds of flows under consideration is identical and hence, we present the methodology for relativistic flow only. For a given set of input parameters, namely, $\mathcal{E}$, λ, and a_k, we calculate the critical point location by solving Eqs. (10), (20), (35), and (36) simultaneously. Since any realistic accretion flow passes through the saddle type critical point only [9,48], in this study, we focus on those accretion solutions that contains saddle type critical points. Accordingly, hereafter we refer to the saddle type critical point as a critical point in the subsequent analysis. When flow possesses multiple critical points, one usually forms very close to the black hole horizon which is called an inner critical point ($r_{\rm in}$) and the other forms far away form the horizon called an outer critical point ($r_{\rm out}$). In this scenario, accretion flow successfully connects the black hole horizon and the outer edge of the disc, as it passes through either the inner or outer critical point. Interestingly, another viable possibility also exists here. Rotating inflowing matter, when it first crosses the outer critical point ($r_{\rm out}$) to become supersonic, it experiences centrifugal repulsion that eventually triggers the centrifugally supported shock transition in the flow variables ([10], and references therein) where supersonic preshock flow jumps in to the subsonic branch of the postshock flow. In the subsonic branch, flow momentarily slows down, however, gradually gains its radial velocity due to the influence of strong gravity, and finally enters into the black hole after passing through the inner critical point ($r_{\rm in}$). Solutions of these kinds are physically accepted and called the shock induced global accretion solutions around the black hole. The position of the shock transition is known as the shock location (r_s) which provides the measure of the size of the postshock corona. In the subsequent sections, we present the elaborate discussion on shock solutions.

In order to understand the transonic nature of the accretion flow, in Fig. 1 we depict the variation of energy ($\mathcal{E}_c$) as a function of the critical point locations (r_c). In the figure, the critical points are plotted in logarithmic scale while the energy is plotted in linear scale. Solid, dotted, and dashed curves represent the results corresponding to relativistic flow, semirelativistic flow, and nonrelativistic flow, respectively. Here, we choose $\lambda = 1.90$ and $a_k = 0.99$. We observe that when critical points form at a large distance, the flow energy in all the cases remain the same; however, when critical points form close to the horizon, the flow energy differs considerably at least for the nonrelativistic flow. The small difference in energy between relativistic and semirelativistic flows justifies the adopted approximation that the value of the radial Lorentz factor (γ_v) deviates only slightly from unity for semirelativistic flow. We draw a horizontal dot-dashed line corresponding to $\mathcal{E} = 1.005$ that intersects with all the curves thrice. This indicates that flow with $(\mathcal{E}, \lambda) = (1.005, 1.90)$ possess multiple critical points in all three cases. In fact, it also indicate that for a flow with fixed λ, there is a range $\mathcal{E}_s \le \mathcal{E} \le \mathcal{E}_h$ for which flow possesses three critical points. Needless to mention that both $\mathcal{E}_s$ and $\mathcal{E}_h$, marked in the figure, depend on the λ and a_k, respectively. For $\mathcal{E} > \mathcal{E}_h$, flow possesses only a single critical point and for $\mathcal{E}_{\rm min} < \mathcal{E} \le \mathcal{E}_s$, flow possesses two critical points. When $\mathcal{E} < \mathcal{E}_{\rm min}$, the critical point ceases to exist.

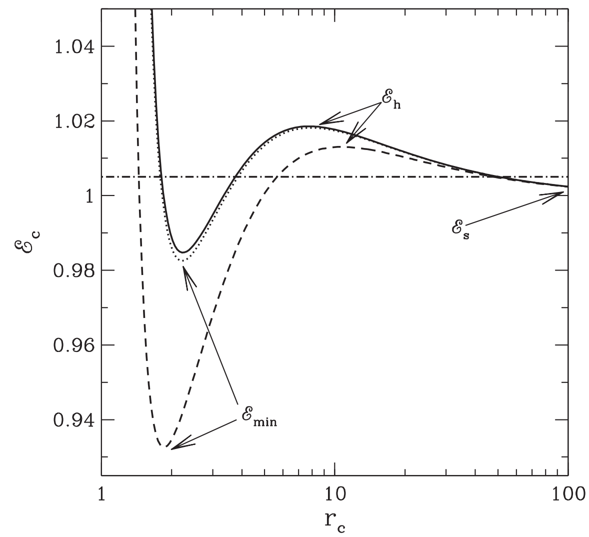

FIG. 1. Variation of energy ($\mathcal{E}_c$) measured at the critical points (r_c) as function of r_c. Solid, dotted, and dashed curves represent the results obtained for R, SR, and NR flows, respectively. Here, we choose $\lambda = 1.90$ and $a_k = 0.99$. See text for details.

B. Procedure to compute global accretion solutions

To obtain a transonic accretion solution, we first calculate the critical point location (r_c) for a given set of input parameters $(\mathcal{E}, \lambda, a_k)$. Afterwards, we employ the critical point conditions [either (35)–(36) or (37)–(38)] to calculate the radial velocity and temperature of the flow at the critical point. These values are used as the initial conditions to integrate the wind equation. In the case of relativistic and semirelativistic flows, we integrate Eq. (22), first staring from the critical point up to very close to the horizon and again from the critical point up to a large distance ($x_{\rm edge}$, equivalently the outer edge of the disc). Eventually, by joining these two parts of the solution, we obtain a global transonic accretion solution around a rotating black hole. In actuality, one would get the identical accretion solution provided the integration of the wind equation is started with the flow variables at $x_{\rm edge}$. For nonrelativistic flows, Eq. (31) is integrated to obtain the transonic accretion solutions.

C. Parameter space for multiple critical points

As already pointed out, depending on the input parameters, an accretion flow may possess multiple critical points. In Fig. 2, we separate the effective domain of the parameter space spanned by $\mathcal{E}$ and λ for global accretion solutions containing multiple critical points. We obtain the result for semirelativistic flow using $a_k = 0.99$. Here, we identify four distinctly different regions of the parameter space named O, A, W, and I, based on the type of the solution topologies. In the insets, we display the representative plots of the global solutions which are obtained for the set of input parameters ($\mathcal{E}$, λ) chosen from these identified regions of the parameter space as marked in the figure. In all the plots, filled circles represent the location of the critical points and arrows indicate the direction of the flow motion corresponding to the smooth global accretion solutions. The result corresponding to the O-type solution is obtained for $(\mathcal{E}, \lambda) = (1.001, 1.86)$ where the outer critical point is located at $r_{\rm out} = 211.5867$. We obtain the A-type solution using $(\mathcal{E}, \lambda) = (1.001, 2.00)$ and a solution of this type contains both inner and outer critical points as $r_{\rm in} = 1.4203$ and $r_{\rm out} = 210.0059$, respectively. Similarly, for the W-type solution, we consider $(\mathcal{E}, \lambda) = (1.004, 2.05)$ and obtain $r_{\rm in} = 1.3372$ and $r_{\rm out} = 60.9931$. Finally, we calculate the I-type solution for $(\mathcal{E}, \lambda) = (1.013, 2.05)$ that only passes through the inner critical point at $r_{\rm in} = 1.3341$. Note that the regions marked A and W provide the global accretion solutions that contain multiple critical points.

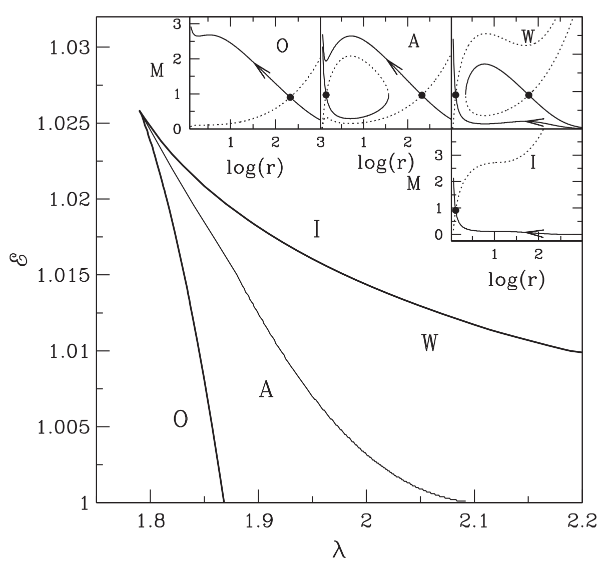

FIG. 2. Division of parameter space in $\lambda - \mathcal{E}$ plane on the basis of flow solutions for semirelativistic flow. Four regions are marked as "O," "A," "W," and "I" and the corresponding representative solutions (variation of Mach number $M = v/C_s$) are depicted in the boxes. In each box, the filled circle represents the location of critical point and the arrow indicates the overall direction of the accretion flow motion. See text for details.

Next, we compare the domain of the parameter space for multiple critical points considering the nature of the flow to be relativistic, semirelativistic, and nonrelativistic, respectively. The comparative study is carried out around nonrotating ($a_k = 0$), moderately rotating ($a_k = 0.5$), and rapidly rotating ($a_k = 0.99$) black holes and the obtained results are depicted in Fig. 3. In each panel of Fig. 3, the effective domain bounded with solid, dotted, and dashed curves are obtained for relativistic, semirelativistic, and nonrelativistic flows and the values of a_k are marked. We observe that parameter spaces for multiple critical points corresponding to relativistic and semirelativistic cases are in agreement irrespective to the black hole spin (a_k) value. However, the parameter space obtained for nonrelativistic flow deviates considerably from the relativistic case and the deviation increases with the increase of a_k. In reality, as a_k is increased, the position of the inner critical points is shifted towards the horizon where space-time is largely distorted and thus the resulting discrepancy is observed. Overall, the above findings clearly indicate that the nonrelativistic approximation bears a noticeable limitation as it fails to describe the accretion flow dynamics around rotating black holes satisfactorily.

D. Global accretion solution containing shock

It is already anticipated (see Sec. IV.A) that an accretion flow can pass through the multiple critical points when flow experiences a discontinuous shock transition in between

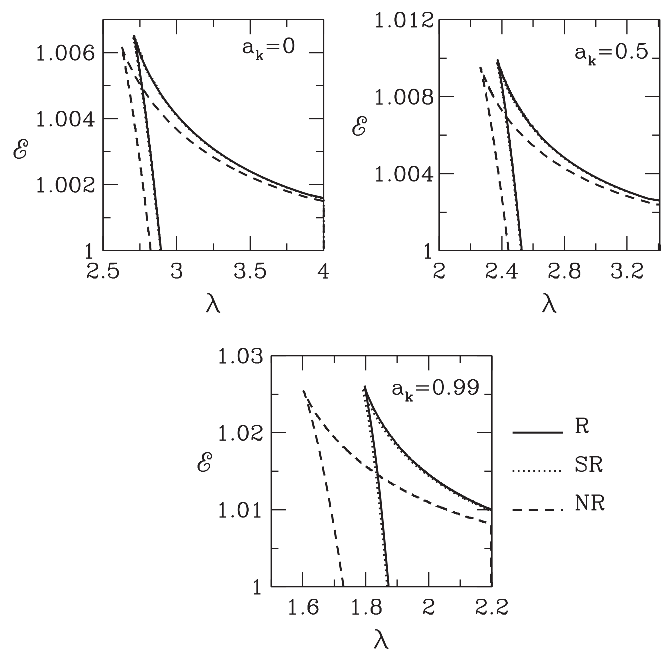

FIG. 3. Comparison of parameter space in the $\lambda - \mathcal{E}$ plane that admits the flow to contain multiple critical points. Regions bounded by solid, dotted, and dashed curves are for R, SR, and NR flows, respectively. The top-left, top-right, and bottom panels are for $a_k = 0.0$, 0.5, and 0.99. See text for details.

them (i.e., $r_{\rm in}$ and $r_{\rm out}$). In general, the formation of shock waves is natural in the astrophysical context ([49–51], and references therein) due to the fact that shock induced accretion solutions possess higher entropy content than the shock free solutions [32]. To compute the shock location, we utilize the relativistic shock conditions which are given by [52],

$$[\rho u^r] = 0, \qquad [(e+p)u^t u^r] = 0, \\ \text{and} \quad [(e+p)u^r u^r + p g^{rr}] = 0, \tag{40}$$

where the difference of quantities across the shock is denoted by the square brackets.

In Fig. 4, we illustrate representative accretion solutions containing multiple critical points where the Mach number ($M = v/C_s$) of the flow is plotted as a function of radial distance. Here, the flow parameters are chosen as $\mathcal{E} = 1.0001$ and $\lambda = 1.989$. Moreover, we consider $a_{\rm k} = 0.99$. The solution consists of two parts passing through two critical points. The one passing through the outer critical point truly establishes the connection between the black hole horizon and the outer edge of the disc, whereas the other one passing through the inner critical point is closed and connects the horizon only. In reality, during the course of accretion process, flow first crosses the outer critical point at $r_{\rm out} = 1022.5621$ and continues to proceed towards the black hole supersonically. Meanwhile, shock conditions are satisfied and flow experiences discontinuous transition at $r_s = 16.5533$. In the figure, the solid vertical arrow indicates the location of a shock transition where flow jumps from the supersonic to subsonic branch. Because of gravity, the subsonic flow gains it radial velocity gradually and eventually enters into the black hole after passing through the inner critical point at $r_{\rm in} = 1.4446$. It may be noted that the accretion flow generally prefers to pass through the shock as the entropy content in the subsonic branch is higher compared to the supersonic branch [32]. The arrows point to the overall motion of the global accretion solution that contains a shock wave. In addition, dotted curves through $r_{\rm in}$ and $r_{\rm out}$ represent the solution corresponding to the wind branch.

In Fig. 5, we compare the shock induced global accretion solutions corresponding to relativistic, semirelativistic, and nonrelativistic flows, respectively. The results depicted in top-left, top-right, and bottom panels are for nonrotating ($a_{\rm k} = 0$), moderately rotating ($a_{\rm k} = 0.5$), and rapidly rotating ($a_{\rm k} = 0.99$) black holes. Here, we consider the energy of the flow as $\mathcal{E} = 1.0001$ for all cases and choose the angular momentum of the flow as $\lambda = 3.15$, 2.75, and 1.989 for $a_{\rm k} = 0$, 0.5, and 0.99, respectively. In each panel, solid, dotted, and dashed curves represent solutions obtained for relativistic, semirelativistic, and nonrelativistic flow and sharp vertical arrows indicate the shock positions.

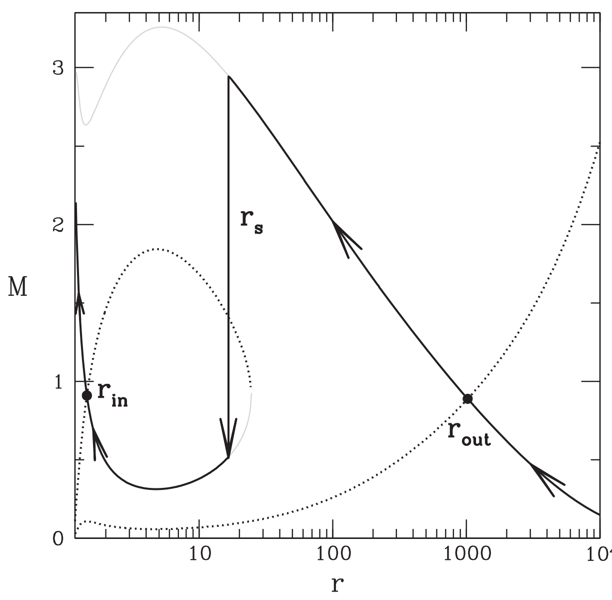

FIG. 4. The Mach number ($M = v/C_s$) of the semirelativistic flow is plotted with radial coordinate (r) for $\mathcal{E} = 1.0001$, $\lambda = 1.989$, and $a_{\rm k} = 0.99$. The thick solid curve represents the accretion solution while the dotted curves refer to the wind solution. The vertical arrow denotes location of shock transition (r_s) and arrows indicate the overall direction of the accretion flow motion. Filled circles refer the critical points where the inner critical point ($r_{\rm in}$) and outer critical point ($r_{\rm out}$) are marked. See text for details.

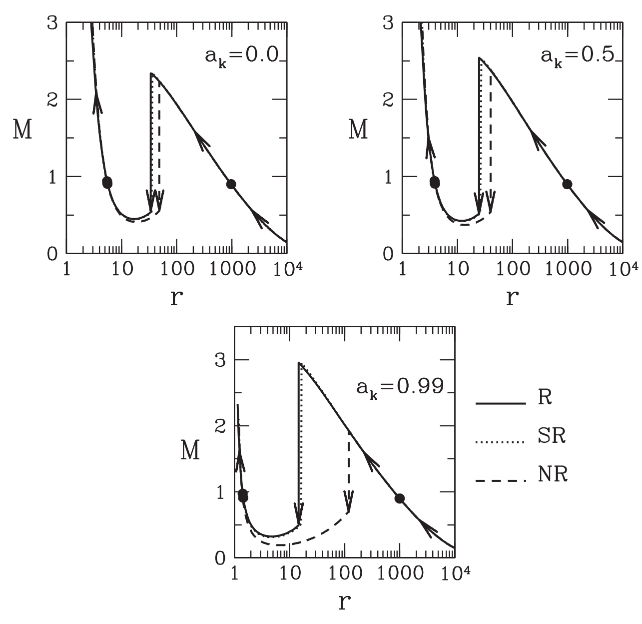

FIG. 5. Comparison of shock induced global accretion solutions obtained from relativistic R (solid), SR (dotted), and NR (dashed) flows. Here, we choose $\mathcal{E} = 1.0001$ and $\lambda = 3.15$ and $a_{\rm k} = 0.0$ for top-left panel, $\mathcal{E} = 1.0001$ and $\lambda = 2.75$ and $a_{\rm k} = 0.5$ for top-right panel and $\mathcal{E} = 1.0001$ and $\lambda = 1.989$ and $a_{\rm k} = 0.99$ for bottom panel. Critical points are shown using filled circles and arrows indicate the direction of flow motion. See text for details.

TABLE I. Comparison of transonic and shock properties. Here, we choose $\mathcal{E} = 1.0001$ for all cases.

a_k	λ		r_{in}	r_{out}	r_s	% Error in r_s
0	3.15	GR	5.5779	998.7680	33.8730	⋯
		SR	5.5674	998.5265	35.9969	6.27
		NR	5.3942	995.6709	48.2825	42.53
0.5	2.75	GR	3.9374	1008.3744	24.6059	⋯
		SR	3.9284	1008.1356	26.6320	8.23
		NR	3.7751	1005.3147	39.8949	62.13
0.99	1.989	GR	1.4485	1022.7973	14.6729	⋯
		SR	1.4446	1022.5621	16.5533	12.81
		NR	1.3496	1019.7915	117.7705	702.63

Moreover, filled circles denote the critical point locations and arrows indicate the overall direction of the accretion flow starting from the outer edge of the disc up to the horizon. Here also we find that the shock locations computed for relativistic and semirelativistic flows are in close agreement and this continues even with the increase of a_k. On the contrary, the obtained shock location for nonrelativistic flow differs noticeably from the relativistic solutions and as before, the amount of deviation is increased with a_k. Quantitative comparison of the transonic and shock properties are given in Table 1.

E. Parameter space for shock

The presence of a shock wave in accretion flow seems to play an important role in determining the black hole spectrum as indicated in [6,53]. Because of the shock transition, postshock flow containing hot and dense electrons inverse Comptonizes the soft photons from the cooled preshock flow and eventually emerges hard radiations. In addition, electrons are energized while crossing the shock front due to the shock acceleration mechanism and produce a nonthermal spectrum. Since shocks are viable and directly involved in deciding the spectral properties of the black hole sources, it is therefore worthy to examine whether the shock solutions discussed in the previous section are isolated solutions or not. For that, we continue the study of shock induced global accretion solutions and make an attempt to accomplish the range of flow parameters that admit shocks. The obtained results are displayed in Fig. 6, where we identify the boundary in the $\lambda - \mathcal{E}$ plane that encompasses the effective region of the parameter space for shock around rotating black holes and separate it from the shock free region. Here, we compute the shock parameter space considering nonrotating ($a_k = 0.0$), moderately rotating ($a_k = 0.5$), and rapidly rotating ($a_k = 0.99$) black holes and they are marked in the figure. The region bounded with solid, dotted, and dashed curves represent the results obtained for relativistic, semirelativistic, and nonrelativistic flows, respectively. We observe that shock parameter space shifts towards the lower angular momentum and higher energy domain as a_k is increased. This happens due to the spin-orbit coupling term in Kerr geometry. We notice that the shock parameter spaces of relativistic and semirelativistic flows are in excellent agreement, but the parameter space computed for nonrelativistic flow does show significant deviation from the relativistic result and the deviation increases with a_k. In particular, for $a_k = 0.99$, the common overlap of the parameter spaces is seen to be marginal. With this, we argue that nonrelativistic approximation for studying the accretion flow dynamics around rotating black hole seems to be incongruous.

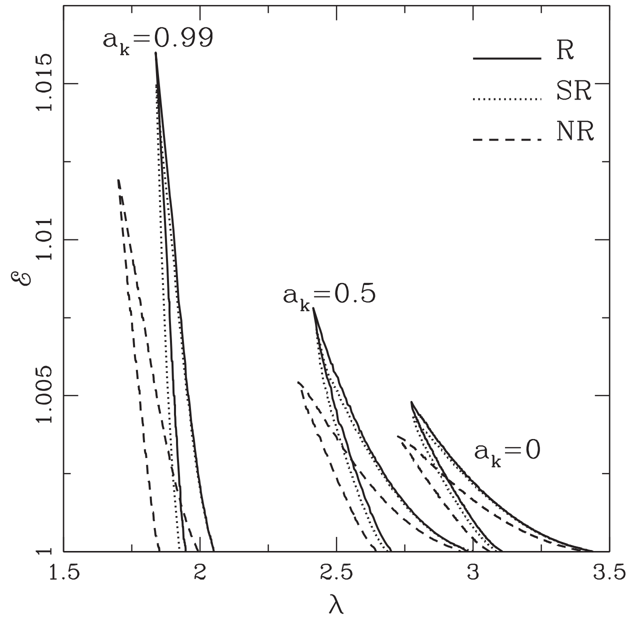

FIG. 6. Comparison of shock parameter space in the $\lambda - \mathcal{E}$ plane. Solid, dotted, and dashed curves represent the results obtained from R, SR, and NR flows. Here, chosen a_k values are marked. See text for details.

V. CONCLUSIONS

In this work, we first formulate the set of hydrodynamic equations that describe the accretion flow in a general axisymmetric background and identify an effective potential $\Phi^{\rm eff}$ [see Eqs. (11a) and (11b)]. Subsequently, we consider the disc to be confined on the equatorial plane (i.e., $\theta = \pi/2$) and investigate the behavior of relativistic accretion flow around the Kerr black hole. Further, since the radial velocity of the accreting matter, in general, remains within a few percent of the speed of light even in the vicinity of the horizon (i.e, $r > 4r_g$), we assume $\gamma_v \rightarrow 1$ all throughout the flow. With this consideration, which is named as the semirelativistic limit, we continue to study the accretion flow around the rotating black hole. It is to be noted that the equations of mass conservation and entropy generation are not affected by this semirelativistic approximation. In addition, we also explore the possibility, where both radial velocity and thermal energy are small as

$v \ll 1$ and $h(r) \sim 1$, and this scenario is referred to as the nonrelativistic limit. Finally, we compare the results for the aforementioned three different approaches. It is noteworthy that the effective potential remains unaltered due to the assumptions adopted in those approaches and it is calculated as

$$\Phi_e^{\mathrm{eff}} = 1 + \frac{1}{2}\ln\left[\frac{r\Delta}{a_{\mathrm{k}}^2(r+2) - 4a_{\mathrm{k}}\lambda + r^3 - \lambda^2(r-2)}\right].$$

Below we summarize our findings based on the present work.

(1) We carry out critical point analysis considering relativistic, semirelativistic, and nonrelativistic flows. Excellent agreement is seen between the results obtained from both the relativistic and semirelativistic limit as far as the transonic properties are concerned. However, in the nonrelativistic limit, results deviate significantly (see Fig. 1).

(2) We separate the domain of the parameter space in the $\lambda - \mathcal{E}$ plane based on the nature of solution topologies. We realize that a large region of the parameter space permits the existence of multiple critical points which is one of the main criteria to harbor a shock wave in accretion flow (see Fig. 2). Moreover, we find that parameter spaces for multiple critical points match accurately enough for relativistic and semirelativistic flows, but a profound difference is seen in the case of the nonrelativistic flow and the deviation increases with a_{k} (see Fig. 3).

(3) Considering the semirelativistic flow, we obtain the shock induced global accretion solution around the rapidly rotating black hole (see Fig. 4). Further, we compare the shocked solutions among the relativistic, semirelativistic, and nonrelativistic flows having identical outer boundary conditions. We find that the position of shocks in relativistic and semirelativistic flows agrees well with a deviation of 6%–12% for $0 \le a_{\mathrm{k}} \le 0.99$. But, the difference of the shock position between relativistic and nonrelativistic flows happens to be very large which becomes monumental ($> 62\%$) for the rapidly rotating black hole ($a_{\mathrm{k}} = 0.99$).

(4) We identify the effective region of the parameter space in the $\lambda - \mathcal{E}$ plane that permits the shock transition in relativistic, semirelativistic, and nonrelativistic flows. We observe that shock induced global accretion solutions are not stray solutions; instead, they continue to exist for a large range of flow parameters. Moreover, it has been shown in this paper that the shock parameter space for relativistic and semirelativistic flows do show close matching even when the spin of the black hole is very high ($a_{\mathrm{k}} = 0.99$). But, shock parameter space obtained for nonrelativistic flow does not show any overlap with the relativistic results.

Based on the above findings, we stress that the semirelativistic approximation could be used to study the accretion flow dynamics using the identified effective potential (Φ_e^{eff}). Our claim stems from the fact that the obtained results closely match with the relativistic one as far as the transonic and shock properties are concerned. Moreover, unlike the existing gravitational potentials [18–20,22], this potential does not suffer any limitation due to the choice of the black hole spin as it works seamlessly for $a_{\mathrm{k}} \to 1$. In reality, for all practical purposes, this potential can be successfully incorporated with ease just like a Newtonian potential. In particular, it would be possible to carry out the complete study of accretion flow including nonlinearities such as shock transitions even in the presence of viscous dissipation, radiative cooling, and magnetic fields around extremely rotating black holes. Since the oscillations of shocks are known to exhibit the quasiperiodic oscillations (QPOs) of the emergent high energy radiations (i.e., hard x rays), and the QPO frequency is linked as $\nu_{\mathrm{QPO}} \sim 1/t_{\mathrm{infall}}$, where t_{infall} refers to the free fall time from the shock position, and the origin of the high frequency QPO can be examined as shocks usually form closer to the rapidly rotating black holes [54]. Moreover, the precise interpretations of the spectral and timing properties of the hard radiations emanating from the accretion flows, which in turn depend on shock, would be viable and subsequently would enable one to constrain the spin of the rapidly rotating black holes ([55], and references therein). At the end, the most important point we would like to bring to the reader's notice is that our analysis enables one to carry out the numerical simulations of accretion flow around rapidly rotating black hole very easily simply by replacing (a) the existing approximate Newtonian and/or pseudo-Newtonian potentials by more accurate potential Φ_e^{eff} obtained through full general relativistic consideration and (b) $\rho^{-1}(dp/dr)$ by $(h\rho)^{-1}(dp/dr)$ in the radial momentum equation. In the forthcoming efforts, we would like to take up all the above tasks that will be reported elsewhere.

APPENDIX A: CALCULATION OF $\frac{dv}{dr}|_{\mathrm{c}}$ FOR RELATIVISTIC FLOW

The gradient of radial velocity at the critical point is given by

$$\left.\frac{dv}{dr}\right|_{\mathrm{c}} = -\frac{-B \pm \sqrt{B^2 - 4AC}}{2A}. \tag{A1}$$

The explicit expressions of A, B, and C are obtained as follows:

$$A = \gamma_v^2\left[1+\frac{2C_s^2}{\Gamma+1}\left\{\frac{1}{v^2}-\frac{A'\Theta_{22}}{v}\right\}\right],$$

$$B = -\frac{2C_s^2\gamma_v^2A'}{(\Gamma+1)v}\Theta_{11}-\frac{2C_s^2}{\Gamma+1}(N_{11}+N_{12})A'\Theta_{11},$$

$$C = -(N_{21}+N_{22}+N_{23}+N_{24}+N_{25}+N_{26}),$$

$$N_{11}=\frac{(r-a_{\mathrm{k}}^2)}{r\Delta}+\frac{5}{2r},\qquad N_{12}=-\frac{1}{2\mathcal{F}}\frac{d\mathcal{F}}{dr},\qquad N_{21}=\frac{2(r-1)}{(r-2)^2r^2},\qquad N_{22}=-\frac{4a_{\mathrm{k}}\lambda\gamma_\phi^2}{r^3\Delta}-\frac{2a_{\mathrm{k}}\lambda\gamma_\phi^2\Delta'}{r^2\Delta^2}+\frac{4a_{\mathrm{k}}\lambda\gamma_\phi\gamma_\phi{}'}{r^2\Delta},$$

$$N_{23}=-\frac{8a_{\mathrm{k}}^2\gamma_\phi^2}{(r-2)r^3\Delta}-\frac{4a_{\mathrm{k}}^2\gamma_\phi^2\Delta'}{(r-2)r^2\Delta^2}+\frac{8a_{\mathrm{k}}^2\gamma_\phi\gamma_\phi{}'}{(r-2)r^2\Delta}-\frac{4a_{\mathrm{k}}^2\gamma_\phi^2}{(r-2)^2r^2\Delta},$$

$$N_{24}=\Omega\gamma_\phi^2\lambda\frac{2a_{\mathrm{k}}^2-(r-3)r^2\Delta'}{r^2\Delta^2}-\gamma_\phi^2\lambda\frac{2a_{\mathrm{k}}^2-(r-3)r^2\Omega'}{r^2\Delta}-2\lambda\Omega\gamma_\phi\frac{2a_{\mathrm{k}}^2-(r-3)r^2\gamma_\phi{}'}{r^2\Delta}$$
$$+2\lambda\Omega\gamma_\phi^2\frac{2a_{\mathrm{k}}^2-(r-3)r^2}{r^3\Delta}+\lambda\Omega\gamma_\phi^2\frac{r^2+2(r-3)r}{r^2\Delta},$$

$$N_{25}=\frac{2a_{\mathrm{k}}(2a_{\mathrm{k}}^2-(r-3)r^2)\Omega\gamma_\phi^2\Delta'}{(r-2)r^2\Delta^2}-\frac{2a_{\mathrm{k}}(2a_{\mathrm{k}}^2-(r-3)r^2)\gamma_\phi^2\Omega'}{(r-2)r^2\Delta}-\frac{4a_{\mathrm{k}}(2a_{\mathrm{k}}^2-(r-3)r^2)\Omega\gamma_\phi\gamma_\phi{}'}{(r-2)r^2\Delta}$$
$$+\frac{2a_{\mathrm{k}}(2a_{\mathrm{k}}^2-(r-3)r^2)\Omega\gamma_\phi^2}{(r-2)^2r^2\Delta}+\frac{4a_{\mathrm{k}}(2a_{\mathrm{k}}^2-(r-3)r^2)\Omega\gamma_\phi^2}{(r-2)r^3\Delta}-\frac{2a_{\mathrm{k}}(-r^2-2(r-3)r)\Omega\gamma_\phi^2}{(r-2)r^2\Delta},$$

$$N_{26}=\frac{2C_s^2}{\Gamma+1}[N_{111}+N_{121}+(N_{11}+N_{12})A'\Theta_{11}],$$

$$N_{111}=-\frac{r-a_{\mathrm{k}}^2}{r^2\Delta}-\frac{(r-a_{\mathrm{k}}^2)\Delta'}{r\Delta^2}-\frac{5}{2r^2}+\frac{1}{r\Delta},\qquad N_{121}=-4a_{\mathrm{k}}^2r\frac{(a_{\mathrm{k}}^2+r^2)\Delta'-4r\Delta}{(a_{\mathrm{k}}^2+r^2)^4-4a_{\mathrm{k}}^4\Delta^2},$$

$$A'=\frac{1}{\Theta}+\frac{\Gamma'}{\Gamma}-\frac{\Gamma'}{\Gamma+1}-\frac{C_s^2(\Gamma+1)}{\Gamma\Theta},\qquad \Theta_{11}=-\frac{2\Theta}{(N+1)}\left[\frac{(r-a_{\mathrm{k}}^2)}{r\Delta}+\frac{5}{2r}-\frac{1}{2\mathcal{F}}\frac{d\mathcal{F}}{dr}\right],$$

$$\Theta_{22}=-\frac{2\Theta\gamma_v^2}{(N+1)v},\qquad \Omega=\frac{2a_{\mathrm{k}}+\lambda(r-2)}{a_{\mathrm{k}}^2(r+2)-2a_{\mathrm{k}}\lambda+r^3},\qquad \Gamma'=\frac{\partial\Gamma}{\partial\Theta}\quad\text{and}\quad \gamma_\phi'=\frac{\gamma_\phi^3}{2}\lambda\Omega'.$$

Here, all the quantities have their usual meaning.

APPENDIX B: Φ_e^{eff} FOR THE SCHWARZSCHILD BLACK HOLE ($a_{\mathrm{k}}=0$)

For the Schwarzschild black hole ($a_{\mathrm{k}}=0$), the effective potential reduces to

$$\Phi_e^{\mathrm{eff}}|_{a_{\mathrm{k}}=0}=1+\frac{1}{2}\ln\left[\frac{(r-2)r^2}{r^3-\lambda^2(r-2)}\right],=1-\frac{1}{2}\ln[1-x],$$

where $x=2(\frac{\lambda^2}{2r^2}-\frac{1}{r-2})$.

For $-1\le x<1$, we get

$$\Phi_e^{\mathrm{eff}}|_{a_{\mathrm{k}}=0}=1+\frac{2^0}{1}\left(\frac{\lambda^2}{2r^2}-\frac{1}{r-2}\right)+\frac{2^1}{2}\left(\frac{\lambda^2}{2r^2}-\frac{1}{r-2}\right)^2+\frac{2^2}{3}\left(\frac{\lambda^2}{2r^2}-\frac{1}{r-2}\right)^3+\frac{2^3}{4}\left(\frac{\lambda^2}{2r^2}-\frac{1}{r-2}\right)^4+\cdots\cdots,$$

where the second term in the right-hand side of the above equation represents the well-known Paczyński-Wiita effective potential [2].

[1] J. Frank, A. King, and D. J. Raine, *Accretion Power in Astrophysics*, 3rd ed. (Cambridge University Press, Cambridge, 2002).
[2] B. Paczyński and P. J. Wiita, Astron. Astrophys. **88**, 23 (1980), http://adsabs.harvard.edu/abs/1980A%26A....88..23P.
[3] M. A. Abramowicz and W. H. Zurek, Astrophys. J. **246**, 314 (1981).
[4] P. A. Becker and T. Le, Astrophys. J. **588**, 408 (2003).
[5] S. K. Chakrabarti, Astrophys. J. **347**, 365 (1989).
[6] A. Chakrabarti and L. G. Titarchuk, Astrophys. J. **455**, 623 (1995).
[7] S. K. Chakrabarti, Astrophys. J. **464**, 664 (1996).
[8] B. Czerny and M. Elvis, Astrophys. J. **321**, 305 (1987).
[9] S. Das, Mon. Not. R. Astron. Soc. **376**, 1659 (2007).
[10] I. K. Dihingia, S. Das, and S. Mandal, Mon. Not. R. Astron. Soc. **475**, 2164 (2018).
[11] J. Fukue, M. Tojyo, and Y. Hirai, Publ. Astron. Soc. Jpn. **53**, 555 (2001).
[12] J. F. Hawley and Krolik, Astrophys. J. **548**, 348 (2001).
[13] T. Manmoto, S. Mineshige, and M. Kusunose, Astrophys. J. **489**, 791 (1997).
[14] R. Matsumoto, S. Kato, J. Fukue, and A. T. Okazaki, Publ. Astron. Soc. Jpn. **36**, 71 (1984), http://adsabs.harvard.edu/abs/1984PASJ...36...71M.
[15] R. Narayan, S. Kato, and F. Honma, Astrophys. J. **476**, 49 (1997).
[16] B. Sarkar and S. Das, Mon. Not. R. Astron. Soc. **461**, 190 (2016).
[17] R. Yang and M. Kafatos, Astron. Astrophys. **295**, 238 (1995), http://adsabs.harvard.edu/abs/1995A%26A...295..238Y.
[18] I. V. Artemova, G. Bjoernsson, and I. D. Novikov, Astrophys. J. **461**, 565 (1996).
[19] S. K. Chakrabarti and R. Khanna, Mon. Not. R. Astron. Soc. **256**, 300 (1992).
[20] S. K. Chakrabarti and S. Mondal, Mon. Not. R. Astron. Soc., **369**, 976 (2006).
[21] R. I. Ivanov and E. M. Prodanov, Phys. Lett. B **611**, 34 (2005).
[22] B. Mukhopadhyay, Astrophys. J. **581**, 427 (2002).
[23] O. Semerák and V. Karas, Astron. Astrophys. **343**, 325 (1999), http://adsabs.harvard.edu/abs/1999A%26A...343..325S.
[24] B. Aschenbach, Memorie della Società Astronomica Italiana **81**, 319 (2010), http://adsabs.harvard.edu/abs/2010MmSAI..81..319A.
[25] L. Gou, J. E. McClintock, J. Liu, R. Narayan, J. F. Steiner, R. A. Remillard, J. A. Orosz, S. W. Davis, K. Ebisawa, and E. M. Schlegel, Astrophys. J. **701**, 1076 (2009).
[26] L. Gou, J. E. McClintock, M. J. Reid, J. A. Orosz, J. F. Steiner, R. Narayan, J. Xiang, R. A. Remillard, K. A. Arnaud, and S. W. Davis, Astrophys. J. **742**, 85 (2011).
[27] R. M. Ludlam, J. M. Miller, and E. M. Cackett, Astrophys. J. **806**, 262 (2015).
[28] J. Liu, J. E. McClintock, R. Narayan, S. W. Davis, and J. A. Orosz, Astrophys. J. **719**, L109 (2010).
[29] R. Shafee, J. E. McClintock, R. Narayan, S. W. Davis, L.-X. Li, and R. A. Remillard, Astrophys. J. **636**, L113 (2006).
[30] I. Fouxon and Y. Oz, Phys. Rev. Lett. **101**, 261602 (2008).
[31] S. Bhattacharyya, S. Minwalla, and S. R. Wadia, J. High Energy Phys. 08 (2009) 059.
[32] P. A. Becker and D. Kazanas, Astrophys. J. **546**, 429 (2001).
[33] I. K. Dihingia, S. Das, and S. Mandal, Journal of Astrophysics and Astronomy **39**, 6 (2018).
[34] J. Fukue, Publ. Astron. Soc. Jpn. **39**, 309 (1987), http://adsabs.harvard.edu/abs/1987PASJ...39..309F.
[35] K. Fukumura and S. Tsuruta, Astrophys. J. **611**, 964 (2004).
[36] R. Kumar and I. Chattopadhyay, Mon. Not. R. Astron. Soc. **443**, 3444 (2014).
[37] J.-F. Lu, W.-M. Gu, and F. Yuan, Astrophys. J. **523**, 340 (1999).
[38] L. Rezzolla and O. Zanotti, *Relativistic Hydrodynamics* (Oxford University Press, Oxford, 2013).
[39] R. H. Boyer and R. W. Lindquist, Journal of Mathematical Physics **8**, 265 (1967).
[40] J. Peitz and A. Appl, Mon. Not. R. Astron. Soc. **286**, 681 (1997).
[41] H. Riffert and H. Herold, Astrophys. J. **450**, 508 (1995).
[42] I. Chattopadhyay and D. Ryu, Astrophys. J. **694**, 492 (2009).
[43] S. Chandrasekhar, *An Introduction to the Study of Stellar Structure* (University of Chicago Press, Chicago, 1939).
[44] J. P. Cox and R. T. Giuli, *Principles of Stellar Structure, Vol. 2: Applications to Stars* (Gordon and Breach, New York, 1968).
[45] J. L. Synge, *The Relativistic Gas* (North-Holland Publishing Co., Amsterdam, 1957).
[46] B. Sarkar, S. Das, and S. Mandal, Mon. Not. R. Astron. Soc. **473**, 2415 (2018).
[47] E. P. T. Liang and K. A. Thompson, Astrophys. J. **240**, 271 (1980).
[48] S. K. Chakrabarti and S. Das, Mon. Not. R. Astron. Soc. **349**, 649 (2004).
[49] S. K. Chakrabarti, *Theory of Transonic Astrophysical Flows* (World Scientific, Singapore, 1990).
[50] K. Schaal and V. Springel, Mon. Not. R. Astron. Soc. **446**, 3992 (2015).
[51] K. Schaal, V. Springel, R. Pakmor, C. Pfrommer, D. Nelson, M. Vogelsberger, S. Genel, A. Pillepich, D. Sijacki, and L. Hernquist, Mon. Not. R. Astron. Soc. **461**, 4441 (2016).
[52] A. H. Taub, Phys. Rev. **74**, 328 (1948).
[53] S. Mandal and S. K. Chakrabarti, Astsron. Astrophys. **434**, 839 (2005).
[54] R. Aktar, S. Das, and A. Nandi, Mon. Not. R. Astron. Soc. **453**, 3414 (2015).
[55] R. Aktar, S. Das, A. Nandi, and H. Sreehari, Mon. Not. R. Astron. Soc. **471**, 4806 (2017).